A&A 410, 639–648 (2003)
DOI: 10.1051/0004-6361:20031212

Astronomy & Astrophysics

Testing the "strong" PAHs hypothesis

II. A quantitative link between DIBs and far-IR emission features

G. Mulas[1], G. Malloci[1,2,⋆], and P. Benvenuti[2,3,⋆⋆]

[1] INAF - Osservatorio Astronomico di Cagliari - AstroChemistry Group, Strada n.54, Loc. Poggio dei Pini, 09012 Capoterra (CA), Italy
[2] Dipartimento di Fisica, Università degli Studi di Cagliari, S.P. Monserrato-Sestu Km 0.7, 09042 Cagliari, Italy
[3] Space Telescope-European Coordinating Facility, ESA, Karl-Schwarzschild-Strasse 2, 85748 Garching bei Munchen, Germany

Received 15 April 2003 / Accepted 5 August 2003

Abstract. In Paper I (Malloci et al. 2003) we proved the profile invariance of the first permitted electronic transition of the typical Polycyclic Aromatic Hydrocarbon cation $C_{32}H_{14}^{+}$ as a first necessary check for the "strong" PAHs hypothesis. In this paper we derive a quantitative relation between the intensities of the former band, which ought to be observable in absorption in the visible range, and those of the far-IR bands, which are predicted by the PAH model to be simultaneously present in emission. Contrary to the mid-IR bands, collectively known as "Unidentified Infrared Bands" (UIBs), which do not discriminate specific molecules, the far IR, skeletal bands can be expected to be a fingerprint of each single species. This fact provides a number of independent constraints which must be simultaneously fulfilled for a successful PAH identification. Our approach thus offers a powerful criterion for the identification of specific PAHs, both in the presently available ISO data and in those of the forthcoming SIRTF and Herschel missions. As an interesting by-product, we quantitatively evaluate the impact of isotopic substitutions ($^{13}C \rightarrow ^{12}C$ and D $\rightarrow$H) on the resulting infrared emission bands.

Key words. astrochemistry – line: identification – molecular processes – ISM: lines and bands – ISM: molecules – infrared: ISM

1. Introduction

The so called "Unidentified Infrared Bands" (UIBs) are emission bands seen in the infrared near 3030, 1610, 1280, 1150 and 885 cm^{-1} (3.3, 6.2, 7.7, 8.6 and 11.3 μm), in numerous galactic objects as well as in external galaxies. First detected in two planetary nebulae by Gillett et al. (1973), UIBs have since been ubiquitously observed in dusty environments along a large number of interstellar sight-lines covering a wide range of excitation conditions (see e.g. Allamandola et al. 1989).

UIBs are commonly believed to arise from the vibration of CH and CC bonds in aromatic groups, hence their other common name of "Aromatic Infrared Bands" (see e.g. Pech et al. 2002). Their most natural interpretation is in terms of free gas phase polycyclic aromatic hydrocarbons (PAHs) which are thought to be ubiquitous in the interstellar medium thanks to their high photostability and the fact that they are carbon-based (Léger & Puget 1984; Allamandola et al. 1985). The physical mechanism invoked for the production of the UIBs is the IR-cooling of PAHs transiently heated by the absorption of a single UV/visible photon (see e.g. Léger & Puget 1984; Allamandola et al. 1985, 1989; Puget & Léger 1989).

In order to understand the role of PAH compounds in the chemistry of the interstellar medium (ISM) it is necessary to identify individual members in this class. This task is far from trivial on the sole basis of the oserved UIBs, because the near and mid infrared region contains most of the normal vibrational modes which are a common, shared feature of the whole class of PAHs (Langhoff 1996); this is supposed to be the reason why these features are so strong, since a whole population of different PAH-like molecules may contribute to them. Indeed, in order to match to the observational constraint of smooth profiles of the observed bands, a mixture of radicals, neutrals and ionized molecules is required, rather than a single such species. Along these lines, recent laboratory IR spectra of neutral and positively charged PAHs, have been successfully used by Allamandola et al. (1999) to model the observed UIBs. For this same reason therefore these same near and mid infrared bands do not permit an unambiguous identification of any single molecular species (Langhoff 1996; Salama 1999). However, on the other hand, every single such molecule ought to show its spectral fingerprint both in the far infrared spectral regions, which contains the vibrational frequencies

Send offprint requests to: G. Mulas, e-mail: gmulas@ca.astro.it
⋆ e-mail: gmalloci@ca.astro.it.
⋆⋆ e-mail: pbenvenu@eso.org.

associated with the bending of the skeletal structure (Langhoff 1996; Zhang et al. 1996; Joblin et al. 2002), and UV/visible electronic transitions. Hence UIBs ought to be strongly related to the diffuse interstellar bands (DIBs), and their possible common root represents the so-called PAHs-DIBs hypothesis in its most ambitious form (see e.g. Salama 1999 and references therein). Indeed, as shown by Rouan et al. (1992) and quantitatively studied in Mulas (1998) and Malloci et al. (2003), infrared emission is supposed to be the dominant mechanism driving the rotation of an isolated PAH in the ISM, hence suggesting a direct link between DIB spectral profiles and IR emission bands.

Following the above line of reasoning to its extremes, it is clear that if PAHs account for the UIBs, their electronic transitions *must* also show up in the form of a large number of DIBs (Léger & D'Hendecourt 1985; van der Zwet & Allamandola 1985). Therefore the failure to find their absorption bands in the visible would cast strong doubts on the applicability of the PAHs model for the UIBs and on their alleged presence in the ISM at all: the two hypotheses are not unrelated and independent but, instead, they either stand together or fail together.

As a matter of fact, despite many observational, experimental and theoretical efforts which led to infer upper limits on the abundance of some PAHs (see e.g. Salama & Allamandola 1992a,b; Ehrenfreund et al. 1995), no definitive spectral identification of any specific interstellar PAH exists to date. The identification of DIBs-UIBs would thus yield an important improvement in our knowledge of the physics and chemistry of the ISM. First of all, since the abundances of dust forming elements, such as carbon, required by any dust model seem to be larger than those available in the ISM, the identification of some large, carbon-bearing molecule, and the resulting measure of its column density, would place direct constraints on the well-known problem of the "carbon-crisis" (Cardelli et al. 1996). More broadly, it would have an impact on our understanding of the origin of life on the early Earth through the exogenous delivery (cometary encounters and meteoritic bombardments) of prebiotic organic molecules (see e.g. Bernstein et al. 1999).

In Malloci et al. (2003), henceforth Paper I, we modelled the photophysics of a prototypical medium sized PAH cation, namely $C_{32}H_{14}{}^{+}$, and showed that its vibronic bands can easily match the observational constraint of spectral profile stability of DIBs in a wide variety of interstellar environments. Here we used the same model to obtain its expected IR emission spectra in the same environments, providing a quantitative estimate of the ratio of the equivalent width of the modelled "DIB" and the intensities of the infrared emission bands which ought to be simultaneously produced by the same molecules.

Ovalene ($C_{32}H_{14}$) is a good representative of middle sized, compact PAHs, hence many of the results which we obtained can be expected to apply to other, similar molecules. We can trivially tailor our model to many other large molecules under relatively weak assumptions, so that the present implementation should be regarded as a "proof of concept" for its validity as a diagnostic tool. For this reason, we restricted the present work to neutral ovalene and its singly charged cation, although middle sized PAHs are expected to be significantly present in a wider variety of charge states in many interstellar environments (see e.g. Bakes et al. 2001a,b, and references therein). This does not affect the validity of the results presented here, since infrared emission by free-flying interstellar PAHs is expected to be pumped by single-photon absorption and is thus utterly independent of the history of the molecule considered. We do plan to apply this same approach to a wide range of molecules in this class, including e.g. larger molecules, different hydrogenation and ionisation states, possibly nitrogen substituted species, in forthcoming works.

The general assumptions of the Monte-Carlo model, the parameters it needs and the different ambient interstellar conditions assumed, are fully detailed in Paper I. The present work concentrates on the quantitative link between the modelled "DIB" at about 9700 Å (Ruiterkamp et al. 2002), and the expected infrared emission bands, with particular regard to the skeletal vibrational modes, peculiar of the specific molecule considered (Langhoff 1996; Zhang et al. 1996; Joblin et al. 2002).

Moreover, using the vibrational analysis obtained through ab initio density functional theory calculations, we quantitatively studied the impact of the most likely isotopic substitutions ($^{13}C \rightarrow {}^{12}C$ and $D \rightarrow H$) on the infrared emission bands.

In the following Sect. 2 we present the results of our Monte-Carlo/ab initio approach. We discuss them in Sect. 3 with special emphasis to the new *quantitative* constraint provided for PAHs identification in the ISM. Our main conclusions are presented in the final Sect. 4.

2. Results

In Paper I we used a compendium of calculated and experimental data about $C_{32}H_{14}$ and $C_{32}H_{14}^{+}$ to run our Monte-Carlo model (Mulas 1998) for a grid of molecular parameters and exciting radiation fields. In particular, the four different radiation fields considered are shown in Fig. 1.

All our ab initio calculations were performed using the NWChem computer code (Harrison et al. 2001). Following Langhoff (1996); Bauschlicher & Langhoff (1997), and Hudgins et al. (2001) we obtained the full vibrational analysis using density functional theory, specifically with the exchange-correlation functional B3LYP (Becke 1993; Stephens et al. 1994) and the 4-31G Gaussian basis set (Frish et al. 1984) to expand the molecular orbitals. According to the table of characters of the D_{2h} point group, the $132 (3 \times 46 - 6)$ normal modes of vibration of $C_{32}H_{14}$ and $C_{32}H_{14}^{+}$ span the following irreducible representation (see e.g. Wilson Jr. et al. 1955, p. 327):

$$\begin{aligned}\Gamma_{132} \;=\; & 23A_g + 10A_u + 22B_{1g} + 12B_{1u} \\ & + 9B_{2g} + 22B_{2u} + 12B_{3g} + 22B_{3u},\end{aligned} \tag{1}$$

where the molecule is assumed to lie in the $x-y$ plane.

2.1. Absolute IR fluxes

We obtained all of the 132 vibrational frequencies for both the neutral and ovalene cation at the ground state optimised geometry using the usual projection operator technique

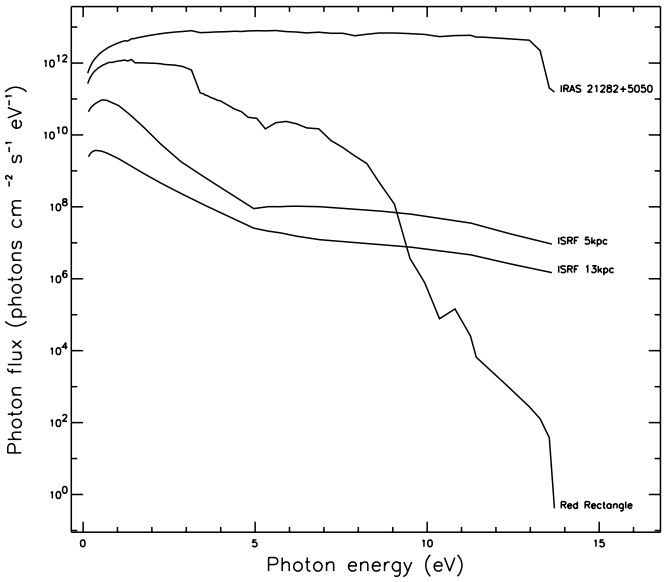

Fig. 1. Two average interstellar radiation fields of Mathis et al. (1983), 5 kpc and 13 kpc away from the galactic centre are compared to the radiation fields of the stars illuminating the specific reflection and planetary nebulae considered in this work; both of them were obtained from stellar atmospheric models of Kurucz (1992) scaled by the blackbody dilution factor corresponding to the geometry of the source (cf. Paper I).

(Wilson Jr. et al. 1955) implemented within NWChem. They are all used within the Monte-Carlo model to compute the density of vibrational states as a function of energy. The complete list of the 56 IR-active modes (symmetries B_{1u}, B_{2u} and B_{3u}), the corresponding symmetries, the vibrational type (CC stretch, CH bend etc.) and the absolute intensities of the corresponding 0−1 transitions of $C_{32}H_{14}$ and $C_{32}H_{14}{}^{+}$ can be found in Malloci (2003). The vibrational frequencies obtained through quantum-chemical calculations at the B3LYP/4-31G level of theory are well known to slightly overestimate the real values for this class of molecules, and are usually scaled with an empirical factor of ∼0.958, which accounts for anharmonicity (Langhoff 1996; Bauschlicher & Langhoff 1997; Hudgins et al. 2001) and brings them into near coincidence with experimental data. Our calculated vibrational frequencies are in good agreement with the results previously published by Langhoff (1996). However, to avoid introducing empirical parameters, we chose to use the vibrational frequencies exactly as obtained by our quantum-chemical calculations, with no scaling; this is consistent with our long-term aim to build a complete theoretical computational machine, capable to run with as few free parameters as possible.

For more details on the grid of adopted parameters which we ran our Monte-Carlo model on, we again refer the reader to Paper I, while the algorithm of the model is fully described in Mulas (1998).

Our Monte-Carlo model yields the IR emission bands produced by the IR-cooling cascades following the absorption of a sequence of UV/Vis photons (see Paper I). More specifically, the model outputs the total power $\mathcal{P}$ isotropically radiated in each IR-active vibrational mode by one molecule embedded in a given radiation field. The dimensions of this quantity are energy per unit time per unit solid angle. We obtained the expected absolute IR emission spectra of both $C_{32}H_{14}$ and $C_{32}H_{14}^{+}$. In particular, we present here only the results obtained using the approximation (a) of the absorption cross section of the cation in the vacuum ultraviolet, as defined in Paper I following Robinson et al. (1997); the results we obtained using approximation (b) from the same reference are virtually undistinguishable in the present context.

Tables 3 and 4 list the predicted $\mathcal{P}$ values respectively for the neutral and cation molecule in all of the different interstellar radiation fields considered here. Band positions are given in μm, and the results of simulations are given in terms of flux, integrated over the given band, per unit column density of the emitting species, in units of W sr^{-1}. Band positions are reported as calculated by the NWChem ab initio quantum chemistry package, with no empirical scaling. They are estimated to be accurate within a few percent. Their relative positions are expected to be more accurate, hence we list them with enough significant digits to distinguish close bands.

For readability, we also depict the resulting emission spectra respectively in Figs. 3 and 4, where we used a fixed band width of 0.1 μm in order to make sure that peak heights be proportional to band fluxes. We stress that our results are the absolute integrated fluxes (i.e. the Tables 3 and 4), since we have no new information about band-widths, which were arbitrarily chosen in order to maximize readability of the synthetic spectra (i.e. the Figs. 3 and 4), which are meant to be nothing more than a concise and convenient representation.

2.2. Isotopic substitutions

Thanks to the fact that our computational approach uses ab initio calculations to perform the vibrational analysis of the species under study, we could easily estimate the effects of isotopic substitutions on the resulting IR emission spectra.

The vibrational analysis in the case of isotopic substitutions can be obtained with no additional computational costs, reusing the hessian previously computed for the unsubstituted case. In $C_{32}H_{14}$ there are respectively 9 inequivalent C atoms and 4 inequivalent H atoms; they are labelled in Fig. 2. Table 1 lists the multiplicity of each inequivalent atom and the corresponding statistical weight, i.e. the estimated probability of it being singly replaced respectively by ^{13}C or D, as obtained for the abundances given by Wilson & Rood (1994) and assuming no isotopic fractionation. We evaluated the overall probabilities considering substitutions as cumulative independent binomial events. More specifically, assuming the probability of each single substitution to be proportional to the isotopic abundances, $p_1 = {}^{13}\mathrm{C}/{}^{12}\mathrm{C} \simeq 1/70$ and $p_2 = \mathrm{D/H} \simeq 1.6{\times}10^{-5}$, we obtained:

$$P(0,32;p_1) \simeq 0.6310, \quad P(0,14;p_2) \simeq 0.9998,$$
$$P(1,32;p_1) \simeq 0.2926, \quad P(1,14;p_2) \simeq 0.0002,$$
$$P(2,32;p_1) \simeq 0.0657, \quad P(2,14;p_2) < 10^{-7}.$$

We considered only single isotopic substitutions, and not multiple simultaneous ones, since their probabilities turn out to be much smaller.

Table 1. Multiplicities ω of the 13 inequivalent atoms of $C_{32}H_{14}$ labelled in Fig. 2 and corresponding statistical weigth, evaluated from the probabilities of $p^* = 0.631$ and $q^* = 0.002$ for ^{12}C and H to be replaced by their most aboundant isotopes ^{13}C and D, respectively.

Inequivalent atom	Multiplicity ω	Statistical weight
1	2	$1/16 \cdot p^*(1-q^*)$
3	4	$1/8 \cdot p^*(1-q^*)$
7	4	$1/8 \cdot p^*(1-q^*)$
11	4	$1/8 \cdot p^*(1-q^*)$
15	4	$1/8 \cdot p^*(1-q^*)$
19	4	$1/8 \cdot p^*(1-q^*)$
23	4	$1/8 \cdot p^*(1-q^*)$
27	2	$1/16 \cdot p^*(1-q^*)$
29	4	$1/8 \cdot p^*(1-q^*)$
33	2	$1/7 \cdot q^*(1-p^*)$
35	4	$2/7 \cdot q^*(1-p^*)$
39	4	$2/7 \cdot q^*(1-p^*)$
43	4	$2/7 \cdot q^*(1-p^*)$

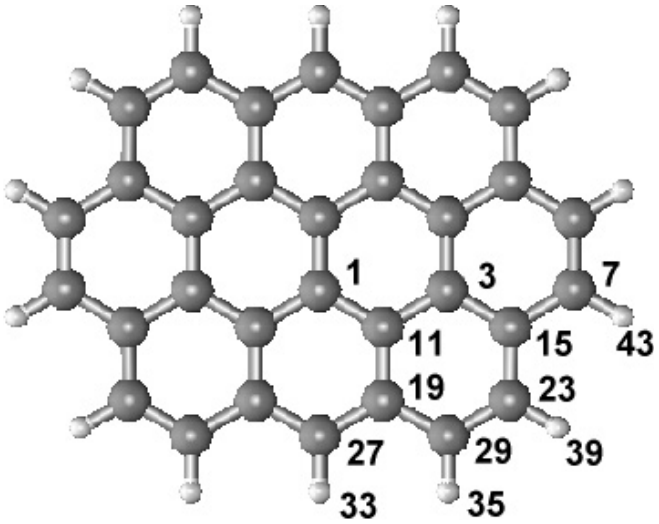

Fig. 2. Ground state geometry of $C_{32}H_{14}$ showing the 9 inequivalent C atoms (labelled by 1, 3, 7, 11, 15, 19, 23, 27 and 29) and the 4 inequivalent H atoms (labelled by 33, 35, 39 and 43); the molecule lies in the *xy*-plane, the *y*-axis being the longer one.

Of course, since isotopic substitutions lower the symmetry of the molecule, a large number of bands which are IR-inactive in the unsubstituted molecule become weakly active. However, these single isotopic substitutions produce a negligible effect on the overall predicted band *intensities*. The lengthy, complete list of the estimated $\mathcal{P}$ in every IR-active band, for all the radiation fields considered and each of the inequivalent single isotopic susbtitutions is presented in Malloci (2003), and it is not reproduced here.

On the other hand, these substitutions may affect in a possibly detectable way the predicted spectral profiles of some single bands. Figures 5–7 show details of selected spectral regions around the strongest bands. In each figure, the top box presents respectively the IR spectrum for no isotopic substitutions and for each of the 13 inequivalent isotopic substitutions labelled in Fig. 2; the bottom box shows the overall expected spectrum, obtained as a weighted sum of the above spectra with statistical weights according to Table 1, along with the spectrum obtained with no isotopic substitutions, for comparison.

Note that we did not model the intrinsic profile of specific bands, which has been studied in detail in the literature (see, e.g. Verstraete et al. 2001; Pech et al. 2002) but just arbitrarily assumed sensible values for their widths, with the aim to emphasize the effect of isotopic substitutions alone on the resulting overall profile.

3. Discussion

Our results bring out a quantitative link between the visible absorption bands and the IR emission features.

Under optically thin conditions, the observed integrated flux $\mathrm{d}F_{\rm obs}/\mathrm{d}\Omega$ in a given IR band, per unit solid angle on the sky, is given by

$$\frac{\mathrm{d}F_{\rm obs}}{\mathrm{d}\Omega} = \int \mathrm{d}r\, n(r)\, \mathcal{P}(r), \tag{2}$$

where $n(r)$ is the number density of the emitting species. If the emitting molecules along the line of sight can be assumed to be illuminated by the same radiation field, $\mathcal{P}$ does not depend on r and can be taken out of the integral, hence the above equation simplifies to

$$\frac{\mathrm{d}F_{\rm exp}}{\mathrm{d}\Omega} = \mathcal{N}_{\rm col}\, \mathcal{P}, \tag{3}$$

$\mathcal{N}_{\rm col}$ being the column density of the emitting species. With $\mathcal{N}_{\rm col}$ expressed in cm^{-2} and $\mathcal{P}$ in W sr^{-1}, $\mathrm{d}F_{\rm obs}/\mathrm{d}\Omega$ results expressed in units of W cm^{-2} sr^{-1}.

Analogously, the equivalent width $\mathcal{W}_{\rm DIB}$ of an optically thin vibronic absorption band of central wavelength $\lambda_{\rm DIB}$, a possible DIB, is related to the total column density of absorbers $\mathcal{N}_{\rm col}$ by the well-known formula (see e.g. van der Zwet & Allamandola 1985):

$$\mathcal{W}_{\rm DIB} = \pi\, r_{\rm e}\, \lambda_{\rm DIB}^2\, \mathcal{N}_{\rm col}\, f, \tag{4}$$

where $r_{\rm e} \simeq 2.81794 \times 10^{-13}$ cm is the classical electron radius and f is the oscillator strength of the specific transition considered. Therefore, dividing Eq. (3) by Eq. (4) we obtain the relation

$$\frac{\left(\frac{\mathrm{d}F_{\rm obs}}{\mathrm{d}\Omega}\right)}{\mathcal{W}_{\rm DIB}} = \frac{\mathcal{P}}{\pi r_{\rm e} f \lambda_{\rm DIB}^2}, \tag{5}$$

where all the quantities on the left side are observables, while the right hand side can be evaluated using our model for any "DIB-like" vibronic band of any known molecule and radiation field for which it is applicable. The best way to fully exploit the discriminating power of Eq. (5) is to apply it to spectral features which are peculiar of a single, specific molecular species. While this is certainly the case for the electronic transition of a PAH cation, it is not necessarily so for its near and middle infrared bands, which are typically very similar for the whole class of molecules. The infrared bands which can most safely be expected to be different for each specific molecule

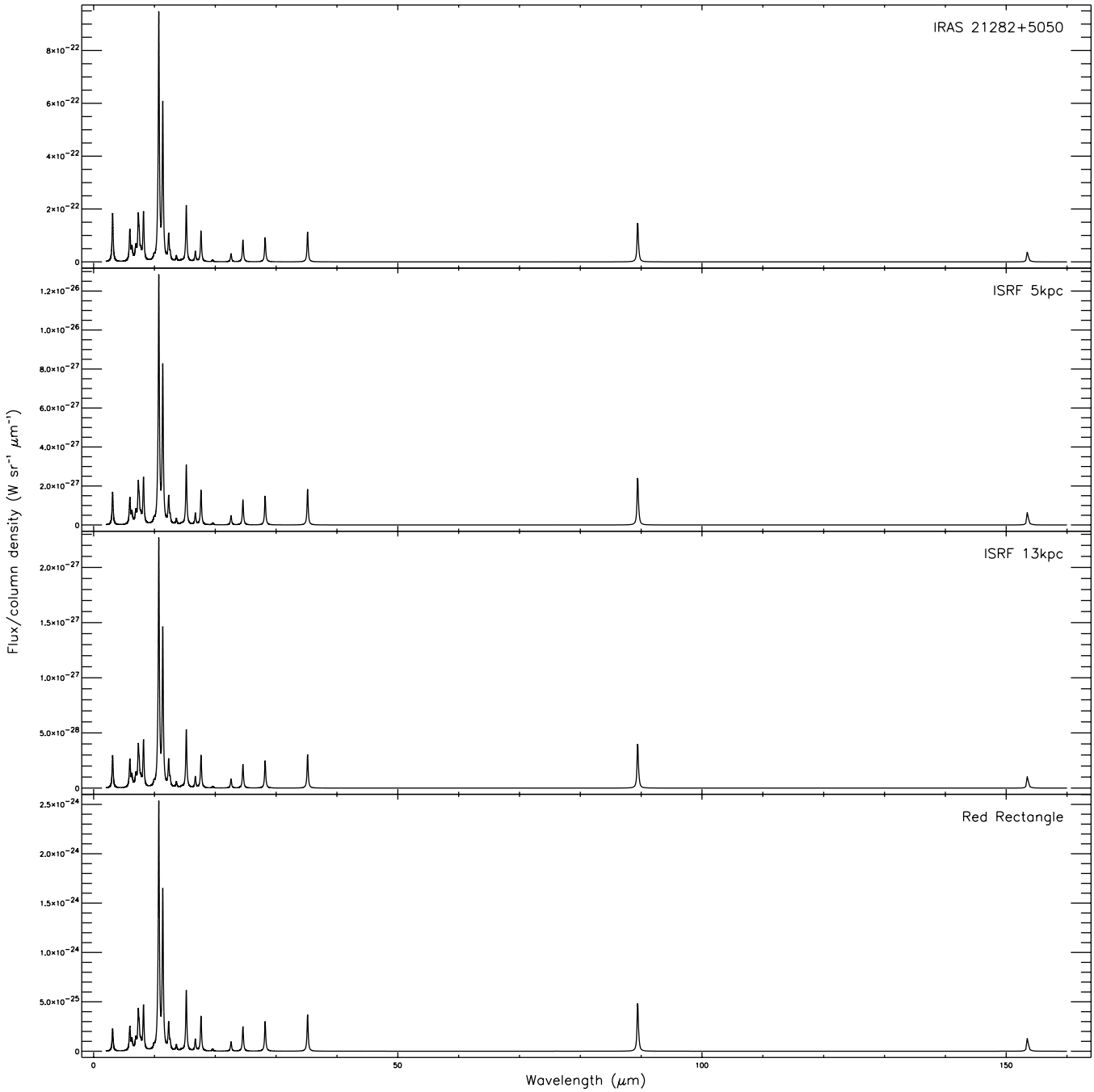

Fig. 3. IR emission spectrum of $C_{32}H_{14}$ in all the radiation fields considered, expressed in terms of flux per unit column density of the emitting species in units of W sr^{-1} μm^{-1}. We arbitrarily assumed a fixed band width of 0.1 μm in order to make sure that peak heights be proportional to band fluxes.

are the ones corresponding to the lowest energy normal vibrational modes, which involve the molecular skeleton in its entirety (Langhoff 1996; Zhang et al. 1996; Joblin et al. 2002). Table 2 shows some numerical values of the right hand side of Eq. (5) obtained considering respectively the two far-infrared skeletal vibrational modes of $C_{32}H_{14}^{+}$ at about 85 and 150 μm and the "DIB" at a wavelength of about 9701 Å, as obtained through our simulation in the four different radiation fields considered, assuming $f \simeq 0.005$ (Ehrenfreund et al. 1995).

Apart from the relation we derived above between the relative intensities of IR emission bands and DIBs, it might be

Table 2. Numerical values of the predicted ratios between $\mathrm{d}F_{\mathrm{obs}}/\mathrm{d}\Omega$ (for the two far-infrared skeletal vibrational modes at about 85 and 150 μm) and $\mathcal{W}_{\mathrm{DIB}}$ of the electronic transition near 9701 Å of $C_{32}H_{14}^{+}$, as obtained through our simulation in the four different radiation fields considered. The ratios in the table are expressed in units of W cm^{-2} sr^{-1} mÅ^{-1}.

IR band position	ISRF 5 kpc	ISRF 13 kpc	Red Rectangle	IRAS 21282 + 5050
83.4 μm	1.3×10^{-16}	1.6×10^{-17}	6.7×10^{-15}	1.4×10^{-11}
150.8 μm	2.9×10^{-17}	3.6×10^{-18}	1.5×10^{-15}	2.9×10^{-12}

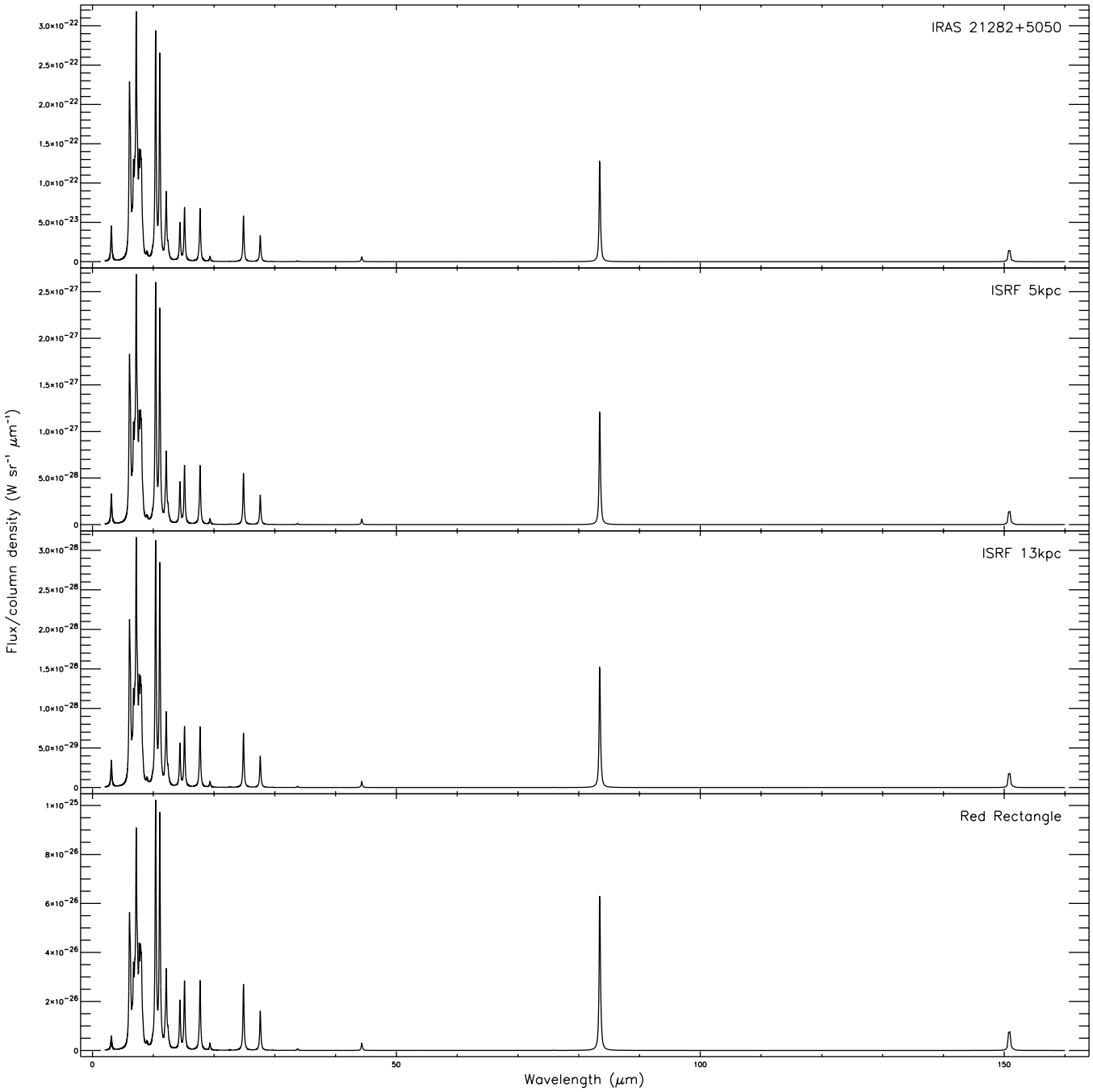

Fig. 4. IR emission spectrum of $C_{32}H_{14}^{+}$ in all the radiation fields considered, expressed in terms of flux per unit column density of the emitting species in units of W sr^{-1} μm^{-1}. We arbitrarily assumed a fixed band width of 0.1 μm in order to make sure that peak heights be proportional to band fluxes.

tempting to consider intensity ratios between different skeletal far-IR bands as possible diagnostics of the radiation field exciting their emission. However, despite the extremely wide variation in the spectra of the radiation fields considered, e.g. between the Red Rectangle and IRAS 21282+5050, and the relatively large frequency difference between the band at ∼85 and ∼150 μm, the predicted intensity ratios remain almost constant, differences being of the order of 1% or less.

Concerning isotopic substitutions, our results show that the resulting isotopic shifts are too small to be resolved in the near and mid infrared bands, with the bandwidths commonly assumed for these bands (see e.g. Pech et al. 2002). Figure 5, for example, shows the expected infrared spectrum of $C_{32}H_{14}^{+}$ in the radiation field of the Red Rectangle, in the wavelength range between about 5 and 9 μm, this time assuming educated guesses for the bandwidths, following Pech et al. (2002). While each single spectrum of the isotopically substituted molecules shows quite apparent differences, their weighted sum according to the expected statistical weights (see Table 1) is virtually undistinguishable from the spectrum of the unsubstituted molecule. Moreover, in the case of near and mid infrared bands it would be very difficult to disentangle the contribution of any

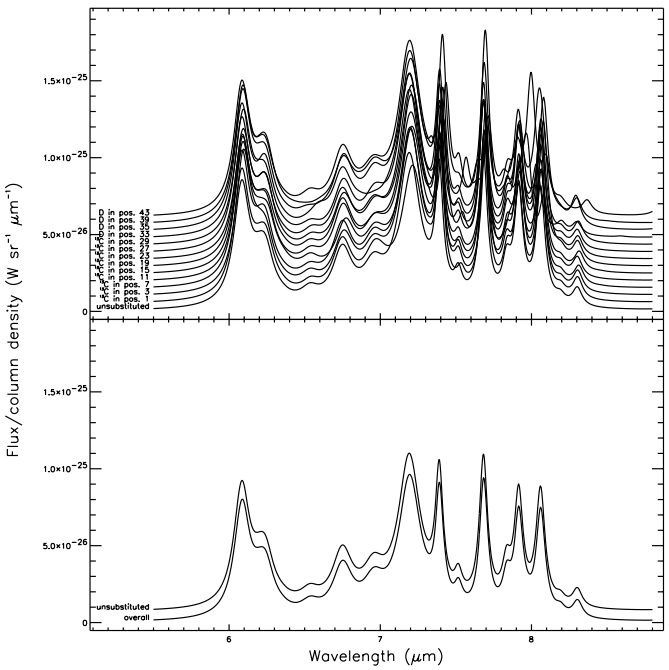

Fig. 5. Expected emission spectrum of $C_{32}H_{14}^{+}$ in the radiation field of the Red Rectangle in the wavelength range between ∼5 and ∼9 μm, assuming educated guesses for the bandwidth following Pech et al. (2002). The top box shows individual spectra for each isotopic substitution, the bottom box compares the spectrum for the unsubstituted molecule with the weighted average assuming standard interstellar isotopic abundances and no fractionation.

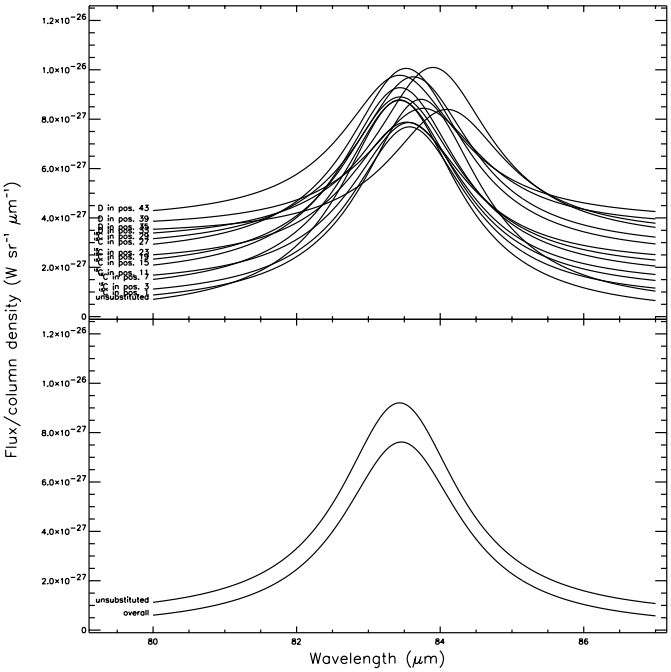

Fig. 6. Expected emission spectrum of $C_{32}H_{14}^{+}$ in the radiation field of the Red Rectangle in the wavelength range around its strongest far infrared skeletal band, near ∼80 μm, assuming a bandwidth of ∼1 μm. The top box shows individual spectra for each isotopic substitution, the bottom box compares the spectrum for the unsubstituted molecule with the weighted average assuming standard interstellar isotopic abundances and no fractionation.

specific molecule (see e.g. Pech et al. 2002) possibly present in many ionisation states (Bakes et al. 2001a,b) and finally, within this contribution, further disentangle the effects of different isotopic substitutions from those of anharmonicity. The situation is more promising for far infrared, skeletal bands, since they are more likely to be able to distinguish different species. However, very little is known on the intrinsic bandwidth of such far-IR bands in PAHs, hence it is difficult to assess whether isotopic substitutions might produce a detectable effect in their profiles. Figures 6 and 7 display again the expected spectrum of $C_{32}H_{14}^{+}$ in the radiation field of the Red Rectangle, this time in the wavelength range around ∼80 μm, for two arbitrarily assumed bandwidths. The comparison between these two figures shows the effect of isotopic substitutions to be definitely visible for a bandwidth of ∼0.1 μm, while it is completely washed out with a bandwidth of ∼1 μm. More detailed experimental measures of far-IR bands in large PAHs are badly needed for a definitive assessment of the importance of isotopic substitutions in this respect.

4. Conclusions and future work

Using ab initio calculations, available experimental data and our Monte-Carlo model, we modelled the photophysics of $C_{32}H_{14}$ and $C_{32}H_{14}^{+}$, obtaining their IR emission bands in a grid of interstellar environments. These results will be useful for a definitive assessment on the presence of such specific molecules in interstellar space.

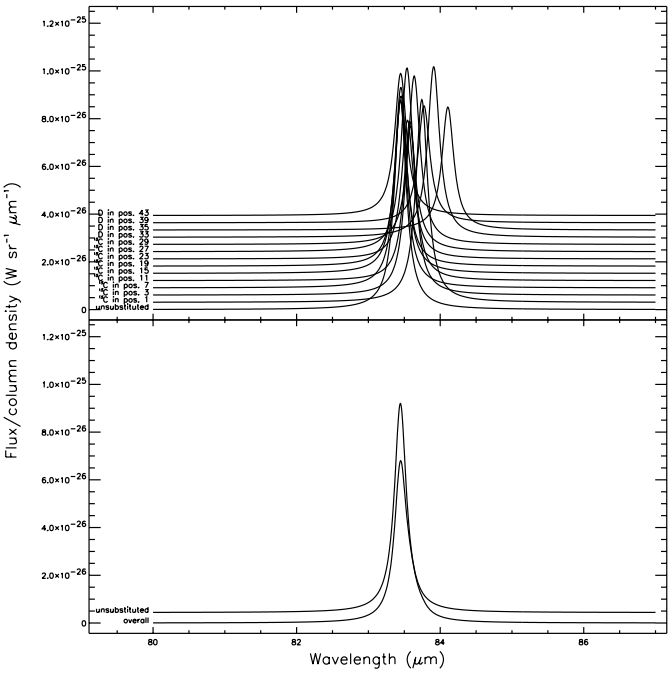

Fig. 7. Expected emission spectrum of $C_{32}H_{14}^{+}$ in the radiation field of the Red Rectangle in the wavelength range around its strongest far infrared skeletal band, near ∼80 μm, assuming a bandwidth of ∼0.1 μm. The top box shows individual spectra for each isotopic substitution, the bottom box compares the spectrum for the unsubstituted molecule with the weighted average assuming standard interstellar isotopic abundances and no fractionation.

Table 3. Values of $\mathcal{P}$, as defined in Sect. 3, for $C_{32}H_{14}$ without isotopic substitutions; bands with a fraction of emitted photons below 0.1% were omitted, leaving 52 out of the 56 IR-active modes of $C_{32}H_{14}$ (cf. Table 5 in Paper I).

Wavelength (μm)	ISRF 5 kpc	ISRF 13 kpc	Red Rectangle	IRAS 21282+5050
3.125	2.8×10^{-28}	4.9×10^{-29}	3.8×10^{-26}	3.1×10^{-23}
3.125	2.2×10^{-28}	3.8×10^{-29}	2.9×10^{-26}	2.4×10^{-23}
3.129	2.0×10^{-29}	3.4×10^{-30}	2.7×10^{-27}	2.1×10^{-24}
3.144	6.3×10^{-31}	1.1×10^{-31}	8.4×10^{-29}	6.7×10^{-26}
3.147	1.2×10^{-29}	2.0×10^{-30}	1.6×10^{-27}	1.3×10^{-24}
3.148	2.3×10^{-29}	4.0×10^{-30}	3.1×10^{-27}	2.5×10^{-24}
3.151	1.1×10^{-29}	1.9×10^{-30}	1.5×10^{-27}	1.2×10^{-24}
5.932	3.1×10^{-28}	5.8×10^{-29}	5.5×10^{-26}	2.7×10^{-23}
5.996	1.8×10^{-28}	3.3×10^{-29}	3.2×10^{-26}	1.5×10^{-23}
6.086	7.8×10^{-30}	1.5×10^{-30}	1.4×10^{-27}	6.8×10^{-25}
6.217	6.6×10^{-30}	1.2×10^{-30}	1.2×10^{-27}	5.7×10^{-25}
6.297	1.8×10^{-28}	3.2×10^{-29}	3.3×10^{-26}	1.5×10^{-23}
6.453	3.1×10^{-29}	5.5×10^{-30}	5.8×10^{-27}	2.6×10^{-24}
6.584	9.5×10^{-30}	1.7×10^{-30}	1.8×10^{-27}	7.8×10^{-25}
6.667	8.5×10^{-30}	1.5×10^{-30}	1.5×10^{-27}	7.0×10^{-25}
6.696	1.6×10^{-32}	2.7×10^{-33}	2.9×10^{-30}	1.3×10^{-27}
6.846	5.6×10^{-29}	9.6×10^{-30}	1.0×10^{-26}	4.6×10^{-24}
6.879	3.8×10^{-29}	6.5×10^{-30}	6.8×10^{-27}	3.1×10^{-24}
6.943	1.5×10^{-29}	2.6×10^{-30}	2.7×10^{-27}	1.2×10^{-24}
6.985	1.5×10^{-28}	2.6×10^{-29}	2.7×10^{-26}	1.2×10^{-23}
7.272	7.0×10^{-29}	1.2×10^{-29}	1.3×10^{-26}	5.7×10^{-24}
7.347	6.0×10^{-28}	1.1×10^{-28}	1.1×10^{-25}	4.9×10^{-23}
7.500	2.9×10^{-28}	4.9×10^{-29}	5.5×10^{-26}	2.2×10^{-23}
7.729	9.0×10^{-29}	1.5×10^{-29}	1.7×10^{-26}	7.0×10^{-24}
7.788	3.5×10^{-29}	5.9×10^{-30}	6.7×10^{-27}	2.7×10^{-24}
7.892	2.2×10^{-29}	3.8×10^{-30}	4.3×10^{-27}	1.8×10^{-24}
8.122	6.5×10^{-29}	1.2×10^{-29}	1.2×10^{-26}	5.0×10^{-24}
8.203	7.5×10^{-28}	1.3×10^{-28}	1.5×10^{-25}	5.8×10^{-23}
8.264	4.3×10^{-30}	7.7×10^{-31}	8.3×10^{-28}	3.3×10^{-25}
9.853	4.8×10^{-30}	9.0×10^{-31}	9.4×10^{-28}	3.9×10^{-25}
9.925	5.4×10^{-29}	1.0×10^{-29}	1.1×10^{-26}	4.4×10^{-24}
10.516	2.1×10^{-28}	3.7×10^{-29}	4.1×10^{-26}	1.5×10^{-23}
10.714	4.3×10^{-27}	7.5×10^{-28}	8.4×10^{-25}	3.1×10^{-22}
11.366	2.7×10^{-27}	4.8×10^{-28}	5.4×10^{-25}	2.0×10^{-22}
12.316	2.9×10^{-28}	5.1×10^{-29}	5.7×10^{-26}	2.1×10^{-23}
12.353	1.8×10^{-28}	3.2×10^{-29}	3.6×10^{-26}	1.3×10^{-23}
12.395	3.7×10^{-31}	6.5×10^{-32}	7.3×10^{-29}	2.7×10^{-26}
12.583	1.1×10^{-28}	2.0×10^{-29}	2.0×10^{-26}	7.6×10^{-24}
13.600	9.7×10^{-29}	1.7×10^{-29}	2.0×10^{-26}	6.9×10^{-24}
14.400	2.0×10^{-29}	3.4×10^{-30}	3.6×10^{-27}	1.2×10^{-24}
14.621	1.2×10^{-29}	2.1×10^{-30}	2.2×10^{-27}	7.5×10^{-25}
15.228	1.1×10^{-27}	1.8×10^{-28}	2.1×10^{-25}	7.3×10^{-23}
16.715	2.0×10^{-28}	3.5×10^{-29}	4.2×10^{-26}	1.3×10^{-23}
17.649	6.2×10^{-28}	1.0×10^{-28}	1.2×10^{-25}	4.0×10^{-23}
17.720	3.6×10^{-30}	6.0×10^{-31}	7.1×10^{-28}	2.3×10^{-25}
19.579	3.3×10^{-29}	4.8×10^{-30}	7.5×10^{-27}	2.3×10^{-24}
22.583	1.6×10^{-28}	2.9×10^{-29}	3.3×10^{-26}	1.0×10^{-23}
24.534	4.5×10^{-28}	7.6×10^{-29}	8.7×10^{-26}	2.9×10^{-23}
28.189	5.4×10^{-28}	9.0×10^{-29}	1.1×10^{-25}	3.3×10^{-23}
35.161	6.7×10^{-28}	1.1×10^{-28}	1.3×10^{-25}	4.1×10^{-23}
89.415	1.1×10^{-27}	1.8×10^{-28}	2.1×10^{-25}	6.5×10^{-23}
153.508	3.5×10^{-28}	5.6×10^{-29}	7.1×10^{-26}	2.0×10^{-23}

Table 4. Values of $\mathcal{P}$, as defined in Sect. 3, for $C_{32}H_{14}^{+}$ without isotopic substitutions; bands with a fraction of emitted photons below 0.1% were omitted, leaving 53 out of the 56 IR-active modes of $C_{32}H_{14}^{+}$ (cf. Table 6 in Paper I).

Wavelength (μm)	ISRF 5 kpc	ISRF 13 kpc	Red Rectangle	IRAS 21282+5050
3.095	4.6×10^{-29}	4.8×10^{-30}	8.3×10^{-28}	6.8×10^{-24}
3.109	3.2×10^{-30}	3.3×10^{-31}	5.7×10^{-29}	4.7×10^{-25}
3.112	7.0×10^{-30}	7.3×10^{-31}	1.2×10^{-28}	1.0×10^{-24}
3.116	2.2×10^{-29}	2.3×10^{-30}	3.9×10^{-28}	3.2×10^{-24}
3.125	7.3×10^{-30}	7.6×10^{-31}	1.3×10^{-28}	1.1×10^{-24}
3.125	1.8×10^{-29}	1.9×10^{-30}	3.2×10^{-28}	2.6×10^{-24}
3.130	2.5×10^{-30}	2.6×10^{-31}	4.5×10^{-29}	3.7×10^{-25}
6.025	1.7×10^{-30}	2.0×10^{-31}	5.1×10^{-29}	2.2×10^{-25}
6.084	5.0×10^{-28}	5.8×10^{-29}	1.5×10^{-26}	6.4×10^{-23}
6.195	8.2×10^{-29}	9.6×10^{-30}	2.5×10^{-27}	1.1×10^{-23}
6.242	1.9×10^{-28}	2.3×10^{-29}	5.9×10^{-27}	2.5×10^{-23}
6.347	1.3×10^{-29}	1.5×10^{-30}	4.3×10^{-28}	1.6×10^{-24}
6.468	1.0×10^{-30}	1.1×10^{-31}	3.2×10^{-29}	1.2×10^{-25}
6.535	5.9×10^{-29}	6.5×10^{-30}	1.9×10^{-27}	6.8×10^{-24}
6.746	1.9×10^{-28}	2.2×10^{-29}	6.3×10^{-27}	2.3×10^{-23}
6.761	6.2×10^{-29}	7.0×10^{-30}	2.0×10^{-27}	7.5×10^{-24}
6.785	2.2×10^{-30}	2.5×10^{-31}	7.3×10^{-29}	2.7×10^{-25}
6.952	9.6×10^{-29}	1.1×10^{-29}	3.1×10^{-27}	1.2×10^{-23}
6.959	5.8×10^{-29}	6.5×10^{-30}	1.9×10^{-27}	7.0×10^{-24}
6.979	1.1×10^{-29}	1.2×10^{-30}	3.5×10^{-28}	1.3×10^{-24}
7.193	8.0×10^{-28}	9.5×10^{-29}	2.7×10^{-26}	9.7×10^{-23}
7.390	2.2×10^{-28}	2.7×10^{-29}	7.5×10^{-27}	2.7×10^{-23}
7.516	4.1×10^{-29}	4.7×10^{-30}	1.5×10^{-27}	4.8×10^{-24}
7.683	2.7×10^{-28}	3.1×10^{-29}	9.6×10^{-27}	3.2×10^{-23}
7.835	6.8×10^{-29}	8.0×10^{-30}	2.5×10^{-27}	8.1×10^{-24}
7.915	2.2×10^{-28}	2.5×10^{-29}	7.7×10^{-27}	2.6×10^{-23}
8.060	2.4×10^{-28}	2.7×10^{-29}	8.4×10^{-27}	2.8×10^{-23}
8.191	1.7×10^{-29}	1.9×10^{-30}	5.8×10^{-28}	2.0×10^{-24}
8.304	4.0×10^{-29}	4.5×10^{-30}	1.4×10^{-27}	4.8×10^{-24}
8.971	6.0×10^{-30}	8.6×10^{-31}	2.4×10^{-28}	9.3×10^{-25}
8.981	9.1×10^{-30}	1.3×10^{-30}	3.6×10^{-28}	1.4×10^{-24}
9.661	4.1×10^{-32}	5.9×10^{-33}	2.0×10^{-30}	6.9×10^{-27}
9.873	9.0×10^{-30}	1.3×10^{-30}	4.3×10^{-28}	1.5×10^{-24}
10.387	8.6×10^{-28}	1.0×10^{-28}	3.3×10^{-26}	9.9×10^{-23}
10.505	4.0×10^{-29}	4.8×10^{-30}	1.5×10^{-27}	4.6×10^{-24}
11.072	7.6×10^{-28}	9.4×10^{-29}	3.2×10^{-26}	9.0×10^{-23}
11.963	4.3×10^{-29}	5.2×10^{-30}	1.8×10^{-27}	5.0×10^{-24}
12.133	2.4×10^{-28}	3.0×10^{-29}	1.0×10^{-26}	2.8×10^{-23}
12.422	4.1×10^{-29}	5.0×10^{-30}	1.7×10^{-27}	4.7×10^{-24}
12.632	7.7×10^{-30}	8.9×10^{-31}	2.7×10^{-28}	8.2×10^{-25}
14.383	1.5×10^{-28}	1.8×10^{-29}	6.8×10^{-27}	1.7×10^{-23}
14.609	1.1×10^{-30}	1.4×10^{-31}	5.0×10^{-29}	1.2×10^{-25}
15.138	2.1×10^{-28}	2.6×10^{-29}	9.5×10^{-27}	2.4×10^{-23}
16.900	1.5×10^{-30}	1.8×10^{-31}	6.4×10^{-29}	1.5×10^{-25}
17.518	1.5×10^{-29}	1.8×10^{-30}	6.5×10^{-28}	1.5×10^{-24}
17.699	2.2×10^{-28}	2.6×10^{-29}	9.7×10^{-27}	2.4×10^{-23}
19.327	2.1×10^{-29}	2.5×10^{-30}	1.0×10^{-27}	2.3×10^{-24}
24.837	2.0×10^{-28}	2.4×10^{-29}	9.5×10^{-27}	2.1×10^{-23}
27.599	1.1×10^{-28}	1.4×10^{-29}	5.8×10^{-27}	1.2×10^{-23}
33.729	4.4×10^{-30}	5.4×10^{-31}	2.5×10^{-28}	3.9×10^{-25}
44.299	2.2×10^{-29}	2.8×10^{-30}	1.1×10^{-27}	2.4×10^{-24}
83.446	5.3×10^{-28}	6.7×10^{-29}	2.8×10^{-26}	5.7×10^{-23}
150.811	1.2×10^{-28}	1.5×10^{-29}	6.2×10^{-27}	1.2×10^{-23}

More generally, we showed this approach to be feasible, at least, for the whole class of PAH molecules and their cations, and demonstrated its potential in providing a number of independent identification criteria for potential DIB-UIBs carriers. In particular, Eq. (5) provides an independent, very powerful criterion for molecule identification, especially with the presently available ISO data and the forthcoming SIRTF and Herschel missions, which are expected to provide the scientific community with observations of unprecedented sensitivity in the wavelength range where far-IR skeletal vibrations of large PAHs are expected to occur. The importance of such calculations for future astronomical observations is underlined in the recent paper by Joblin et al. (2002) where band profiles and intensities of the low-frequency vibrational modes of the neutral coronene molecule ($C_{24}H_{12}$) are presented.

Our long term aim will be to systematically apply the above analysis to a large sample of astrophysically relevant molecules, with particular emphasis on larger PAHs, in a wide range of ionisation and hydrogenation states, possibly nitrogen substituted. With more computational tools providing Time Dependent DFT becoming more reliable and commonly available (see e.g. Weisman et al. 2003), we expect to be able to obtain ab initio electronic excitation energies and absorption spectra of PAHs, at least up to excitation energies of a few eVs (Hirata et al. 1999; Weisman et al. 2001, 2003). This will provide a completely self-contained computational tool which will be a valuable guide for targeted experiments and observations.

Acknowledgements. The authors thank the referee who helped improve the paper with useful comments. G. Malloci gratefully acknowledges the financial support by INAF - Osservatorio Astronomico di Cagliari. The authors are thankful to Prof. G. Cappellini and Dr. G. Satta for their help with ab-initio methodologies. We acknowledge the High Performance Computational Chemistry Group for using their code: "NWChem, A Computational Chemistry Package for Parallel Computers, version 4.0.1" (2001), Pacific Northwest National Laboratory, Richland, Washington, USA.

References

Allamandola, L. J., Hudgins, D. M., & Sandford, S. A. 1999, ApJ, 511, L115
Allamandola, L. J., Tielens, A. G. G. M., & Barker, J. R. 1985, ApJ, 290, L25
Allamandola, L. J., Tielens, G. G. M., & Barker, J. R. 1989, ApJS, 71, 733
Bakes, E. L. O., Tielens, A. G. G. M., & Bauschlicher, C. W. 2001a, ApJ, 556, 501
Bakes, E. L. O., Tielens, A. G. G. M., Bauschlicher, C. W., Hudgins, D. M., & Allamandola, L. J. 2001b, ApJ, 560, 261
Bauschlicher, C. W., & Langhoff, S. R. 1997, Spectrochim. Acta Part A, 53, 1225
Becke, A. D. 1993, J. Chem. Phys., 98, 5648
Bernstein, M. P., Sandford, S. A., Allamandola, L. J., et al. 1999, Science, 283, 1135
Cardelli, J. A., Meyer, D. M., Jura, M., & Savage, B. D. 1996, ApJ, 467, 334
Ehrenfreund, P., Foing, B. H., D'Hendecourt, L., Jenniskens, P., & Désert, F. X. 1995, A&A, 299, 213
Frish, M. J., Pople, J. A., & Binkley, J. S. 1984, J. Chem. Phys., 80, 3265
Gillett, F. C., Forrest, W. J., & Merrill, K. M. 1973, ApJ, 183, 87
Harrison, R. J., Nichols, J. A., Straatsma, T. P., et al. 2001, NWChem, A Computational Chemistry Package for Parallel Computers, Version 4.0.1
Hirata, S., Lee, T., & Head-Gordon, M. 1999, J. Chem. Phys., 111, 8904
Hudgins, D. M., Bauschlicher, C. W., & Allamandola, L. J. 2001, Spectrochim. Acta Part A, 57, 907
Joblin, C., Toublanc, D., Boissel, P., & Tielens, A. G. G. M. 2002, Mol. Phys., 100, 3595
Kurucz, R. 1992, in The Stellar Populations of Galaxies, ed. B. Barbuy, & A. Renzini, Proc. 149th Symp. IAU (Dordrecht: Kluwer Academic Publishers), 225
Langhoff, S. R. 1996, J. Phys. Chem., 100, 2819
Léger, A., & D'Hendecourt, L. 1985, A&A, 146, 81
Léger, A., & Puget, J. L. 1984, A&A, 137, L5
Malloci, G. 2003, Ph.D. Thesis, Università degli Studi di Cagliari
Malloci, G., Mulas, G., & Benvenuti, P. 2003, A&A, 410, 623 (Paper I)
Mathis, J. S., Mezger, P. G., & Panagia, N. 1983, A&A, 128, 212
Mulas, G. 1998, A&A, 338, 243
Pech, C., Joblin, C., & Boissel, P. 2002, A&A, 388, 639
Puget, J. L., & Léger, A. 1989, ARA&A, 27, 161
Robinson, M. S., Beegle, L. W., & Wdowiak, T. J. 1997, ApJ, 474, 474
Rouan, D., Léger, A., Omont, A., & Giard, M. 1992, A&A, 253, 498
Ruiterkamp, R., Halasinski, T., Salama, F., et al. 2002, A&A, 390, 1153
Salama, F. 1999, in Solid Interstellar Matter: The ISO Revolution, Les Houches Workshop, February 2–6, 1998, ed. L. d'Hendecourt, C. Joblin, & A. Jones (EDP Sciences and Springer-Verlag), 65
Salama, F., & Allamandola, L. J. 1992a, Nature, 358, 42
Salama, F., & Allamandola, L. J. 1992b, ApJ, 395, 301
Stephens, P. J., Devlin, F. J., Chabalowski C. F., & Frisch, M. 1994, J. Phys. Chem., 98, 11623
van der Zwet, G. P., & Allamandola, L. 1985, A&A, 146, 76
Verstraete, L., Pech, C., Moutou, C., et al. 2001, A&A, 372, 981
Weisman, J. L., Lee, T. J., & Head-Gordon, M. 2001, Spectrochim. Acta Part A, 57, 931
Weisman, J. L., Lee, T. J., Salama, F., & Head-Gordon, M. 2003, ApJ, 587, 256
Wilson, T. L., & Rood, R. T. 1994, ARA&A, 32, 191
Wilson Jr., B., Decius, J. C., & Cross, P. C. 1955, Molecular Vibrations – The theory of Infrared and Raman Vibrational Spectra (New York: McGraw-Hill)
Zhang, K., Guo, B., Colarusso, P., & Bernath, P. F. 1996, Science, 274, 582